Hydrophobic, Antireflective, Self-Cleaning, and Antifogging Sol–Gel Coatings: An Example of Multifunctional Nanostructured Materials for Photovoltaic Cells

ARTICLE *in* CHEMISTRY OF MATERIALS · JULY 2010

Impact Factor: 8.35 · DOI: 10.1021/cm100937e

6 AUTHORS, INCLUDING:

Marco Faustini
Pierre and Marie Curie University - Paris 6
39 PUBLICATIONS **451** CITATIONS
SEE PROFILE

Cedric Boissiere
Pierre and Marie Curie University - Paris 6
220 PUBLICATIONS **5,290** CITATIONS
SEE PROFILE

Plinio Innocenzi
Università degli Studi di Sassari
211 PUBLICATIONS **4,748** CITATIONS
SEE PROFILE

David Grosso
Collège de France
206 PUBLICATIONS **8,554** CITATIONS
SEE PROFILE

4406 *Chem. Mater.* **2010,** *22,* 4406–4413
DOI:10.1021/cm100937e

CHEMISTRY OF MATERIALS
Article

Hydrophobic, Antireflective, Self-Cleaning, and Antifogging Sol−Gel Coatings: An Example of Multifunctional Nanostructured Materials for Photovoltaic Cells

Marco Faustini,[†] Lionel Nicole,[†] Cédric Boissière,[†] Plinio Innocenzi,[‡] Clément Sanchez,[†] and David Grosso*[,†]

[†]*Chimie de la Matière Condensée de Paris, UMR UPMC−CNRS 7574, Université Pierre et Marie Curie (Paris 6), Collège de France, 11 place Marcelin Berthelot, 75231, Paris, France, and* [‡]*Laboratorio di Scienza dei Materiali e Nanotecnologie (LMNT), CR-INSTM, Università di Sassari, Palazzo Pou Salid Piazza Duomo 6, 07041 Alghero SS, Italy*

Received April 3, 2010. Revised Manuscript Received June 1, 2010

Antireflective, photocatalytic (self-cleaning), water repellent, and high water-wetting (anti fogging) properties were combined for the first time into a sol−gel coating deposited onto glass substrates. Such an original multifunctional coating was obtained by sol−gel liquid deposition of two successive oxide layers. The first coating is composed of a hybrid methyl-functionalized nanoporous SiO_2 material that exhibits high transparency, high water resistance, close to null water adsorption, and fairly high mechanical stability (transversal Young Modulus: 1.5 GPa). Thickness and refractive index can be controlled by selecting proper chemical and processing conditions so as to adjust the anti-reflectivity properties. The second layer is an ultrathin crystalline TiO_2 nanoperforated layer that was deposited on top of the previous antireflective layer. Its thickness and refractive index were adjusted around 12 nm and $n \approx 1.8$ respectively. This hard TiO_2 top layer acts as a protecting barrier toward mechanical aggressions and assures high water wetting (antifogging) and photocatalysis (self-cleaning) at the surface. Indeed, this bilayer system shows an excellent capability to photodecompose organic species that were adsorbed into the Anti-Reflective (AR) layer porosity. We show that the decomposition of model pollutants takes place inside and on the surface of the layer, which is likely due to diffusion of the pollutants toward TiO_2 and/or diffusion of the radical species toward the pollutants. These systems are easy to produce on a large scale at low cost and exhibit high mechanical and chemical durability. They are thus serious candidates to be used as antireflective, self-cleaning coatings for photovoltaic cells.

1. Introduction

Many efforts have been dedicated to the development of novel technologies associated to photovoltaic cells with the aim of increasing the energetic yields of such green energy production devices. Whatever the type of technology to photogenerate electricity (silicon based or Dye-sensitive Solar Cells (DSC)), there is a need to obtain sustainable optical coatings to allow the maximum solar emission to reach the exiton generating semiconductor junction. Applying an Anti-Reflective (AR) layer, with an optimized refractive index and thickness, on top of a glass top cover of the device can partly solve this issue.[1−3] Most of the time, the coatings are primarily porous silica-based material offering tunable refractive index and thickness with excellent adhesion to the glass surface.[4,5] Unfortunately, pure SiO_2 porous coatings are not stable in water since they are sufficiently soluble to be progressively dissolved by rain. This process is augmented by the presence of the porosity that dramatically increases the surface area of the material.[6] In addition, these pores have hydrophilic surfaces and are small enough to be filled-up with water at relatively low humidity through capillary condensation leading to a dramatic effect on the optical properties and thereby increasing the refractive index and provoking a significant reduction of the antireflective properties. Meanwhile, the presence of accessible pores in the nanometer range favoring the adsorption of pollutants from the out-door environment; the latter causes higher adsorption of contaminants that again lead to a rise of the AR layer refractive index and thus to the loss of its optical function. Water up-take can be considerably reduced by making the pores hydrophobic through the use of alkyl functionalized silica precursors.[7]

*To whom correspondence should be addressed. E-mail: david.grosso@upmc.fr. Fax: 33 (0) 1 44 27 47 69. Phone: 33 (0) 1 44 27 15 30.

(1) Kermadi, S.; Agoudjil, N.; Sali, S.; Tala-Ighil, R.; Boumaour, M. *Thin Films Porous Mater.* **2009**, *609*, 221.
(2) San Vicente, G.; Morales, A.; Gutierrez, M. T. *Thin Solid Films* **2001**, *391*, 133.
(3) Wang, X.; Shen, J. J. Sol-Gel Sci. Technol. **2009**, online published
(4) Das, S.; Roy, S.; Patra, A.; Kumar Biswas, P. *Mater. Lett.* **2003**, *57*, 2320.
(5) Wu, G.; Wang, J.; Shen, J.; Yang, T.; Zhang, Q.; Zhou, B.; Deng, Z.; Bin, F.; Zhou, D.; Zhang, F. *J. Non-Cryst. Solids* **2000**, *275*, 169.
(6) Chowdhury, S. R.; Peters, A. M.; Blank, D. H.A.; ten Elshof, J. E. *J. Membr. Sci.* **2006**, *276*, 276.

Published on Web 07/15/2010

On the other hand, contamination cannot be avoided except if the porosity is made non-accessible to pollutants by applying a hermetic barrier layer. Another alternative solution would be to integrate a photocatalyst species to the optical layer whose role would be to clean the porosity through in situ decomposition of the potential organic contaminants upon natural sunlight activation. One of the most efficient materials for such a purpose is TiO_2 anatase which exhibits a total cutoff at wavelength below 350 nm. It has already proven its efficiency in self-cleaning window glasses.[8,9] However, problems exist because of its high refractive index (i.e., $n = 2.5$), which will dramatically reduce the AR properties of the layer. To reduce n, TiO_2 can be nanoparticles embedded into the AR layer network. In this case, the porosity must be increased so as to counter balance the increase in material optical density, inducing a mechanical weakening and a greater contamination through adsorption in the pores. The second possibility is to successively deposit both materials in the desired structure to obtain independent bilayer systems. Combination of TiO_2 and SiO_2 in the same coating either under mixed phases[10] or under independent stack layers[2,3,5,11] obtained through physical deposition or sol−gel liquid deposition techniques has recently been reported for different types of optical applications. None of these solutions combined hydrophobicity of the inner porosity together with photocatalytic activity located only at the surface, and a perfect control of both layer porous structure and refractive index. In the present work, we describe the preparation, the structure, and the properties of bilayer systems composed of an ultrathin Photo-Active (PA) TiO_2 coating onto the surface of an Anti-Reflective (AR) hybrid silica-based layer. The thickness of the top TiO_2 PA layer must be extremely thin, and its refractive index must be as close as possible to the refractive index of the AR layer so as to preserve as much as possible the optical properties. In addition, it is necessary to reduce the thickness of the AR layer to compensate for the presence of the PA layer.

The AR layer is constituted of a calcined methyl-functionalized SiO_2 matrix, exhibiting hydrophobic porosity with pores in the range of several nm in diameter. It has been prepared by dip-coating glass substrates into a sol−gel solution containing partly hydrolyzed and condensed Tetraethoxysilane (TEOS) and Methyltriethoxysilane (MTEOS) precursors in the presence of (PEO-PPO-PEO) Pluronic F127 block copolymer porogene. After thermal stabilization, the PA layer was deposited onto the previous layer by the same liquid deposition method, but using $TiCl_4$ precursor and PB-*b*-PEO block copolymer. Thicknesses were adjusted between 50 and 160 nm for the AR layers and around 15 nm for the PA layer.[12] The refractive index of the AR layer could be adjusted between 1.16 and 1.33 by varying the F127 content, but it was fixed here at around 1.22 (see Experimental Section). The refractive index of the PA coating was reduced to around 1.8 through the creation of homogeneous and ordered void nanoperforations into the material. The scheme of the bilayer system is shown in Figure 1. The top layer could be seen as an ultrathin membrane containing 20 nm in diameter perforations organized into a hexagonal structure.[13] Structural and chemical characterizations were performed using Environmental Ellipsometric Porosimetry (EEP) techniques, Grazing Incidence X-ray analyses at low and wide angles (GI-SAXS and GI-WAXS), electronic and near-field microcopies, FTIR, and UV−visible transmittance. The bilayer system shows close to 4% increase in transmittance compare to the bare substrate at adjustable wavelength range, excellent water repellence, good mechanical properties, self-cleaning properties, and a stability over 9 months immersion into water (longest tested period). These properties match perfectly with the requirements for the final cover of out-door solar cells; however, it also can be applied for other types of optical devices requiring inner hydrophobicity, anti fogging because of high surface energy, antireflectivity, and photo activity integrated properties.

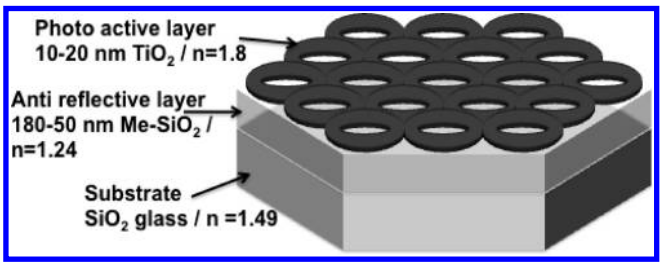

Figure 1. Scheme of the bilayer system composed of the thick AR underneath layer covered by the nanoperforated ultrathin PA layer.

2. Experimental Section

Chemicals. Absolute ethanol was purchased from Normapur while $TiCl_4$, TEOS (TetraEthOxySilane) and MTEOS (MethylTriEthOxySilane) precursors were purchased from Aldrich. F127 Pluronic (EO_{106}-PO_{70}-EO_{106}) and P3017-BdEO PB-b-PEO (polybutadiene-b-polyethyleneoxide, MWPB = 5500 g mol^{-1}, MWPEO = 5000 g mol^{-1}) were purchased from Aldrich and Polymersource respectively.

Anti Reflective Films. AR films were prepared from solutions composed of TEOS/MTEOS/F127/HCl/H_2O/EtOH with respective molar ratio of 0.5:0.5:0.006:0.005:5:40. MTEOS and TEOS were first dissolved in the solution composed of EtOH, HCl (2M) and H_2O before addition of F127; the solution was stirred for at least 2 h before deposition. Films were prepared on silicon and glass microscope slide substrates ($n = 1.49$ at 700 nm) by dip coating at room temperature and at low relative humidity (RH < 5%). The thickness of AR films was tuned using different

(7) Krzyzak, M.; Frischat, G. H.; Hellmold, P. *J. Sol-Gel Sci. Technol.* **2007**, *41*, 99.
(8) Kesmez, O.; Erdem Camurlu, H.; Burunkaya, E.; Arpac, E. *Sol. Energy Mater. Sol. Cell.* **2009**, *93*, 1833.
(9) Zhao, X.; Zhao, Q.; Yu, J.; Liu, B. *J. Non-Cryst. Solids* **2008**, *354*, 1424.
(10) Brinker, C. J.; Harrington, M. S. *Sol. Energy Mater. J.* **1981**, *5*, 159.
(11) Zhang, X. T.; Fujishima, A.; Jin, M.; Emeline, A. V.; Murakami, T. *J. Phys. Chem.B* **2006**, *110*−*50*, 25142.
(12) Faustini, M.; Louis, B.; Albouy, P. A.; Kuemmel, M.; Grosso, D. *J. Phys. Chem.C* **2010**, *114*, 7637.
(13) Kuemmel, M.; Allouche, J.; Nicole, L.; Boissière, C.; Laberty, C.; Amenitsch, H.; Sanchez, C.; Grosso, D. *Chem. Mater.* **2007**, *19*, 3717.

withdrawal rates (1, 2, and 4 mm s^{-1}) keeping all other dip coating conditions fixed. After coating, hybrid films were immediatly calcinated underneath a curing IR lamp at 450 °C for 10 min.

Photo Active Films. PA were obtained from fresh solutions composed of $TiCl_4$/PB-PEO/H_2O/EtOH in the following respective molar proportions: 1:0.002:42:160. A first solution A was prepared by mixing the PB-b-PEO in the water and in 3/4 of the amount of ethanol. Solution A was aged at 70 °C for 2 h until the complete dissolution of the PB-b-PEO and then cooled down at room temperature. A second solution B containing $TiCl_4$ and the remaining ethanol were added to the cooled solution A before being stirred at room temperature for 30 min. PA films were deposited on top of the AR layers by dip coating using a withdrawal speed of 1.5 mm s^{-1} and at a temperature of 40 °C, and relative low humidity. The as-formed bilayer system was then heated at 500 °C for 5 min to ensure crystallization of the TiO_2 top layer. Film samples were labeled as ARX, for the Anti Reflective single layer systems and ARXPA for the Anti Reflective and Photo Active bilayer systems. X stands for the dip-coating withdrawal speed in mm s^{-1} used to prepare the AR layer. Single-side coated samples were obtained by cleaning one side of the substrate prior to heat treatment using a dry tissue imbibed with ethanol.

Film structure was investigated using Field Emission Gun Scanning Electron Microscopy (SEM-FEG) Zeiss Ultra 55, Transmission Electron Microscopy (TEM) JEOL Jem 100CX, and Atomic Force Microscopy (AFM) Veeco DI-CPII in noncontact mode using MPP11123 phosphorus doped silicon probes from Veeco. Grazing Incidence Small-Angle X-ray Scattering (GISAXS-Rigaku S-max 3000 equipped with a microfocus source $\lambda = 0.154$ nm and a 2D Gabriel type detector place at 1480 mm from the sample) was used to assess the structure of the films and the period of the array of PA layer nanoperforations at an angle of incidence of 0.21°. The transmitted and specular reflected beams were masked by a vertical beam-stop. Diffraction patterns were analyzed using Igor software.[14] Ellypsometry measurements were performed on a UV−visible (from 240 to 1000 nm) variable angle spectroscopic ellipsometer (VASE−2000U Woollam), and the data analyses were performed with the Wvase32 software using Cauchy models for both layers. EEP was investigated through capillary condensation of water or toluene into the porosity using an atmospheric control chamber designed by SOPRA-LAB.[19] Photoactivity of the systems was investigated by following the refractive index of the layer, contaminated with Lauric acid, upon UV irradiation. Lauric acid was chosen as model pollutant because it contains hydrophilic and hydrophobic groups found in most organic species. In addition, its carboxylate head and its hydrophobic alkyl tail allow strong interactions to form independently with the TiO_2 (Lewis acid) surface and the hydrophobic inner porosity of the underneath layer, respectively. Finally, if one wants to record the mass loss that is only due to photcatalysis with the present elliposmetry setup, the organic pollutant must absolutely be poorly volatile. The porosity was filled up by impregnation with Lauric acid from a concentrated solution in ethanol. The Lauric acid was deposited by dip-coating at 2 mm s^{-1} the sample into the solution while the filling of the pores was allowed by impregnation inside the porosity because of evaporation-induced capillary filling. The extra Lauric acid deposited on the surface was eliminated using a soft tissue. In this conditions, ellipsometry analysis revealed that the whole porosity was filled with the pollutant while no pollutant layer remains on the surface. The polluted sample was then placed in air at 5 cm under a UV-lamp (365 nm/24W), and optical density was recorded every minute using the previous ellipsometry conditions over a period of 3 days. The UV/vis absorption spectra were recorded by using a UVIKON XL SECOMAM (UVK-Lab) spectrometer directly on the one side coated glass samples. The background was recorded in air only.

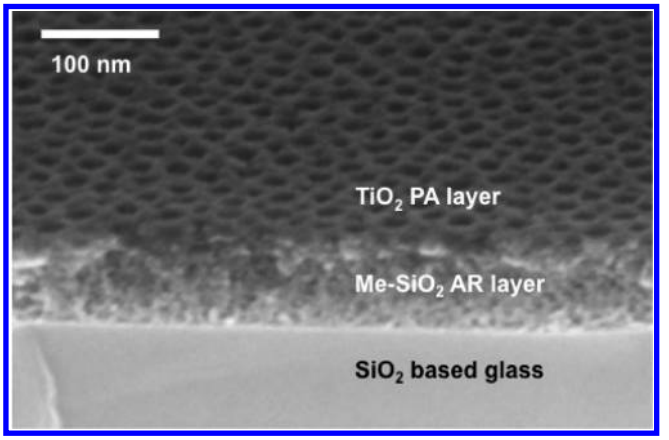

Figure 2. SEM image of the AR2PA bilayer system composed of the thick AR underneath layer covered by the nanoperforated ultrathin PA layer (scale bar = 100 nm).

Fourier Transform Infrared (FTIR) analysis has been performed using a Bruker Vertex70 V spectrophotometer. The optical bench and the sample compartment have been kept in vacuum during the measurement at a pressure lower than 0.5 hPa. The measurements in the middle infrared region have been done using a Globar source, a KBr beamsplitter, and a RT-DLaTGS detector averaging 256 scans with 4 cm^{-1} of resolution. The measures in the far-infrared (FIR) region have been performed using a Globar source, a Si beamsplitter, and a RT-DTGS-FIR detector. The spectra have been recorded in transmission, in the 600−100 cm^{-1} range by averaging 32 scans with 4 cm^{-1} of resolution. A silicon wafer has been used as substrate to measure the background; the baseline has been calculated by a rubberband algorithm (2 iterations, 64 baseline points) (OPUS 7.5 software).

3. Results and Discussion

Figure 2 displays the SEM cross-section image of a typical AR2PA (see Experimental Section for detailed preparation) bilayer system where both AR and PA layers can be independently identified. Indeed, the AR underneath layer has a thickness of several tens of nanometers (difficult to precisely assess as a result of the tilting angle) and is composed of randomly ordered pores of around a few nanometers in diameter. The top TiO_2 layer has a thickness around 10 nm and presents the characteristic nanoperforations of 20 nm in diameter organized into an hexagonal-type compact structure. An ellipsometry investigation of the AR2PA bilayer system confirms that both layers could be independently fitted between 400 and 1000 nm using a non-absorbing Cauchy layer model. Thickness and refractive index at 700 nm were found to be respectively 82 nm and 1.22 for the AR layer and 16 nm and 1.75 for the PA layer, confirming the presence of porosity in both layers. Optical properties of the AR layer were similar before and after the deposition of the PA layer, suggesting that no Ti-oxo-cluster entered the AR layer porosity upon the second

(14) Babonneau, D.; Camelio, S.; Lantiat, D.; Simonot, L.; Michel, A. *Phys. Rev.B* **2009**, *80*, 155446.

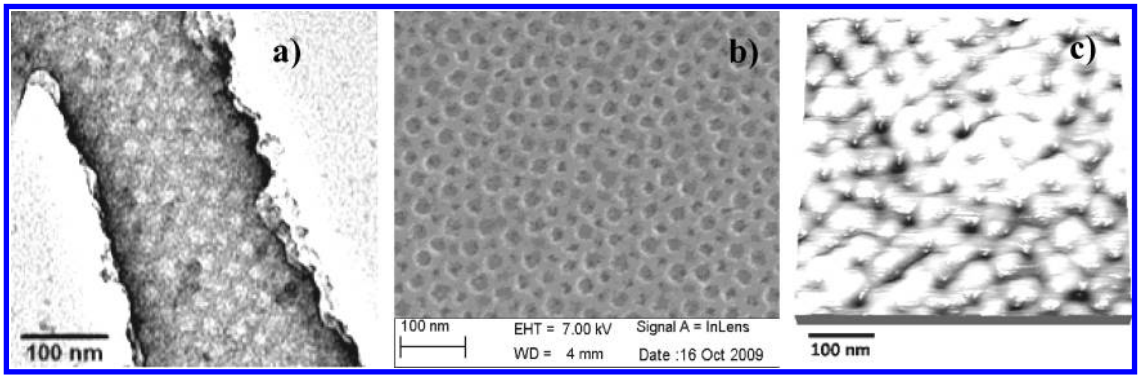

Figure 3. (a) TEM, (b) SEM, and (c) AFM images of the AR2PA bilayer system showing the presence of the 20 nm in diameter nanoperforations at the surface.

dip-coating process. This "impermeability" could be attributed to the hydrophobic porosity and to the low connectivity with the environment (further confirmed by ellipsometry) and also to the fact that PB-b-PEO/Ti-oxo-cluster hybrid micelles are too large to diffuse inside the porosity.

Indeed, PB-*b*-PEO in $EtOH/H_2O$ media forms micelles with the PB in the core and PEO at the shell. Polar PEO units are hydrophilic and have the ability to form strong coordination bonds with Ti (IV) metallic center through interaction between the free electron pairs of O atoms and the vacant d-orbitals of Ti atoms (Lewis acid/base pair). The Ti-oxo-clusters are then expected to remain in the PEO environment together with water. Recent studies[15] show that hybrid Ti-oxo-clusters micelles from a similar PB-b-PEO have an hydrodynamic diameter around 50 nm which are much larger than the pores of the AR layer. They, and their associated coordinated titanium intermediates, do not penetrate the AR layer and remain at the surface to form the nanoperforated PA coating upon thermal treatment. The topography of the bilayer system surface has been also confirmed by TEM, SEM, and AFM investigations as shown in Figures 3.

The TEM image (Figure 3a) shows the TiO_2 hexagonal network, which is darker because of its higher density. The SiO_2-based layer can be seen through the perforations in light gray color. No high resolution or EDX analysis could be performed because of the diffusion of the electronic beam through the AR layer. The SEM-FEG image of the surface (Figure 3b) confirms the structure observed by TEM. The smaller holes, that are visible through the perforations, belong to the underneath AR layer. The perforated topography of the surface is confirmed by AFM topography (Figure 3c). An additional analysis of the AR2PA bilayer system structure is obtained by GI-SAXS and GI-WAXS. Figure 4 displays the GI-SAXS 2D pattern and the GI-WAXS diagram obtained after radial integration of the exposed image plate. In the GI-SAXS pattern, the nanoperforation organization into 2D hexagonal-like structure leads to the presence of the two characteristics diffraction rods at a *d*-spacing of 28 nm (together with their faint harmonic as seen on the intensity profile in the *y* direction (inset Figure 4a)) which corresponds to the (10) planes. The rods are created by the confinement of the diffraction waves into the PA thin layer, and the fact that they are elongated in the vertical direction (normal to the surface) suggests the presence of a single layer of nanoperforation motifs distributed with a similar trend on the whole irradiated surface of the sample. The porous texture of the bottom AR layer should provide a faint diffusion ring at greater *q*-value (marked by white dashed line on the pattern). Such a low intense signal is, however, not observed even on the single AR layer as a result of the poor degree of pore ordering. The WAXS diagram in Figure 4b presents a wide and low intense diffraction signal centered at $2\theta = 24.8°$, confirming the crystallinity of the TiO_2 membrane. Deducing the particle size by applying the Scherrer formula to this diffraction is not appropriate because of the grazing incidence geometry by which the whole width of the sample is irradiated and participates in the construction of the diffraction. A diffraction band, corresponding to the more intense (101) peak of the TiO_2 anatase, is created instead of a real exploitable peak (see Figure 4 inset). One must point out here that irradiated films that are dimensionally longer lead to a wider diffraction band. Here a 7 mm wide sample film and a distance of 60 mm from the detector was used. It seems that the signal is composed of two overlapping but slightly shifted peaks. The diffraction band contains two reinforcements below and above $2\theta = 24.8°$ that correspond to the same anatase phase but are likely due to the higher quantity of material present at the edge of the sample because of typical edge dewetting effects intrinsically associated to the liquid deposition techniques. The low intensity is due to the very low quantity of TiO_2 present on the surface. Crystallization of the PA layer into anatase has been confirmed by the far-infrared absorption spectra in the 510−200 cm^{-1} range (see Figure 5). The spectrum is formed by two intense and well-defined absorption bands, peaking around 436 and 267 cm^{-1}. These vibrational modes are due to transverse optical (TO) E_u phonons in tetragonal anatase with two TiO_2 units per primitive cell.[16,17]

(15) Kuemmel, M.; Smått, J.; Boissière, C.; Nicole, L.; Sanchez, C.; Lindén, M.; Grosso, D. *J. Mater. Chem.* **2009**, *19*, 3638.

(16) Gonzalez, R. J.; Zallen, R.; Berger, H. *Phys. Rev. B* **1997**, *55*, 7014.

(17) Pecharromàn, C.; Gracia, F.; Holdago, J. P.; Ocana, M.; Gonzalez-Elipe, A. R.; Bassas, J.; Santiso, J.; Figueras, A. *J. Appl. Phys.* **2003**, *93*, 4634.

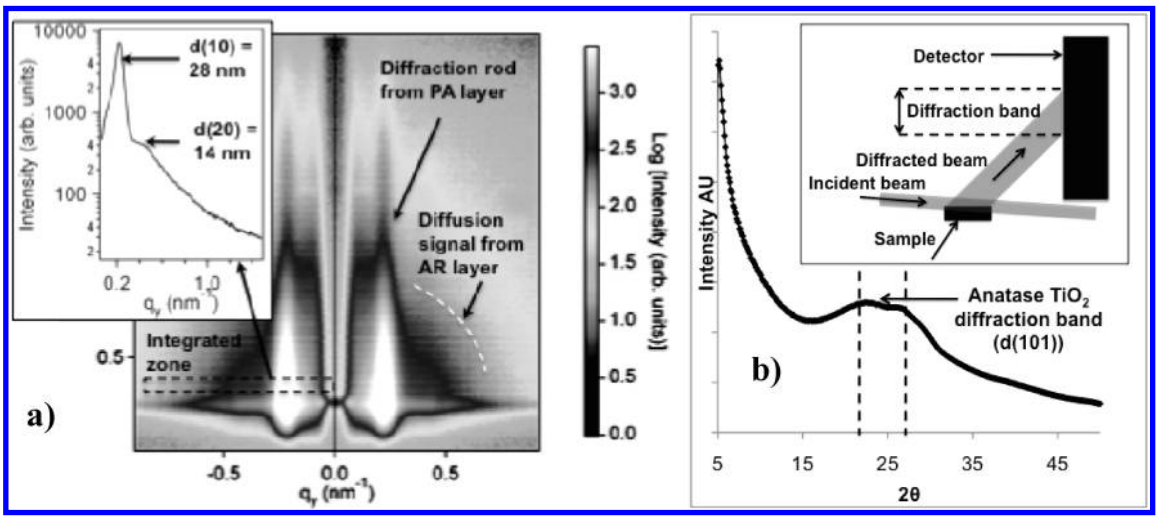

Figure 4. (a) GI-SAXS pattern and (b) GI-WAXS diagram obtained for a typical AR2PA bilayer system.

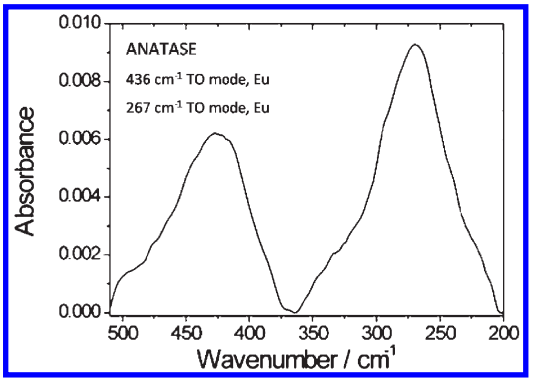

Figure 5. Far infrared absorption spectrum of a titania monolayer obtained on a AR2PA system.

As expected and already observed with the present nanoperforated TiO_2 top layer in a previous study,[18] the deposition of a drop of water on top of the bilayer surface leads to the complete wetting with a contact angle inferior to 10°, confirming the antifogging property of the layer. Such a property is due to the high surface energy of TiO_2.

EEP is a recent and very efficient technique to assess the porosity of an optical coating by probing the adsorption/desorption and capillary condensation of selected vapors inside the film. First, the experiment was performed on the AR layer using water vapor. The sample was exposed to increasing and decreasing relative vapor pressure ($0 < P/P_0 < 1$), and the evolution of refractive index was recorded every $\Delta P/P_0 = 0.02$. The refractive index was found to vary from 1.23 to 1.25 when exposed from 0 to 100% relative humidity (data not shown), suggesting that less than 5% of the porosity can be filled up with condensed water while the rest of the porosity remains empty even at saturated humidity. As already mentioned previously, this behavior is likely due to the presence of residual methyl groups making the surface of the pores hydrophobic. The same film was then aged for 9 months in deionized water, and the same water repellent behavior was observed. The AR layer refractive index and thickness were not modified by the latter treatment, suggesting that the methyl-containing silica framework does not dissolve even after a long period into water. In a second EEP experiment, non-polar toluene vapor was used as adsorbate. In this case, the adsorption/desorption isotherm shows a toluene capillary condensation into the pores suggesting that the porosity is open to the atmosphere. Figure 6a shows a progressive increase of the refractive index of the AR layer with increasing toluene vapor pressure. Capillary condensation for a given P/P_0 value can be related to a specific pore dimension and morphology.[19] In this case, the pore size distribution in Figure 6b) has been obtained from the Kelvin equation using the model describing interconnected pores (cylindrical model) and using the physical and chemical characteristics of toluene.[19] It confirms that a population of pores having diameters below 10 nm are present in the structure. Such a finding is in agreement with the microscopic analysis where pores of various dimensions but below 10 nm in size could be depicted. The desorption branch shows a sudden decrease of the refractive index below 50% that corresponds to the desorption of the toluene. This is characteristic of the "bottle neck" effect, where smaller interconnecting windows assures accessibility to the pores. An important point to underline here is that only non-polar liquids, such as toluene, can condense inside the pores in the studied conditions, which proves that the interface of the pores must be hydrophobic. This hydrophobicity must be associated with uncompleted thermal decomposition of the methyl groups on the surface of the pores, which will be confirmed later by FTIR investigation. For comparison, the same film but free of methyl groups, prepared with 100% TEOS as precursor, shows high hydrophilicity.[19] Mechanical properties of the hybrid AR film were investigated by analyzing the evolution of film thickness in the range of toluene relative pressure for which capillary condensation has occurred ($P/P_0 > 0.6$). Using the Kelvin-Laplace equation given in ref 19 to fit the capillary stress relaxation of the film, we deduced the transverse

(18) Jarn, M.; Brieler, F.; Kuemmel, M.; Grosso, D.; Linden, M. *Chem. Mater.* **2008**, *20*, 1476.
(19) Boissière, C.; Grosso, D.; Lepoutre, S.; Nicole, L.; Brunet-Bruneau, A.; Sanchez, C. *Langmuir* **2005**, *21*, 12362.

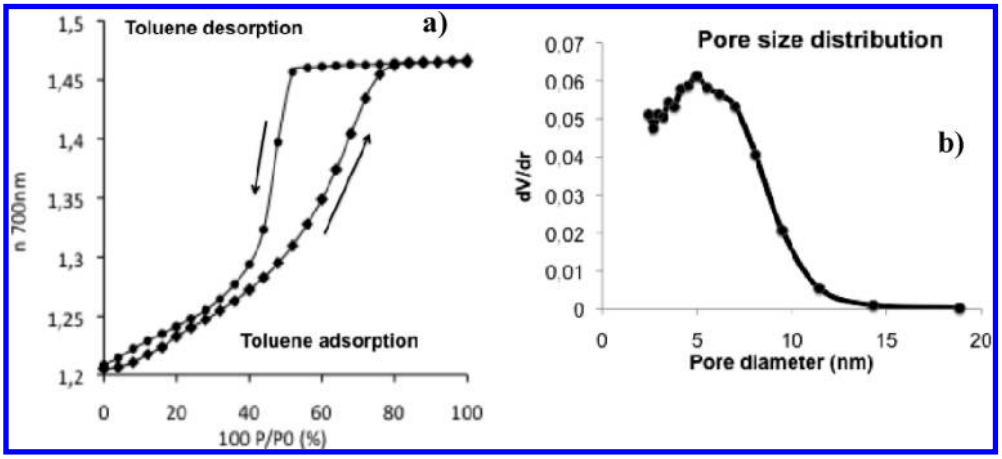

Figure 6. (a) Evolution of refractive index of the AR layer (AR2 sample) upon exposure to increasing and decreasing toluene vapor pressure. (b) Pore size distribution deduced from the adsorption curve.

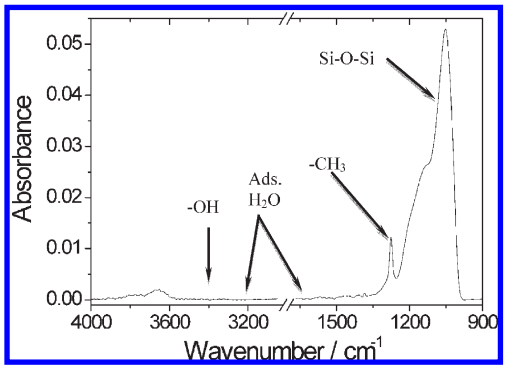

Figure 7. FTIR absorption spectra of a MTES-TEOS hybrid film after thermal treatment.

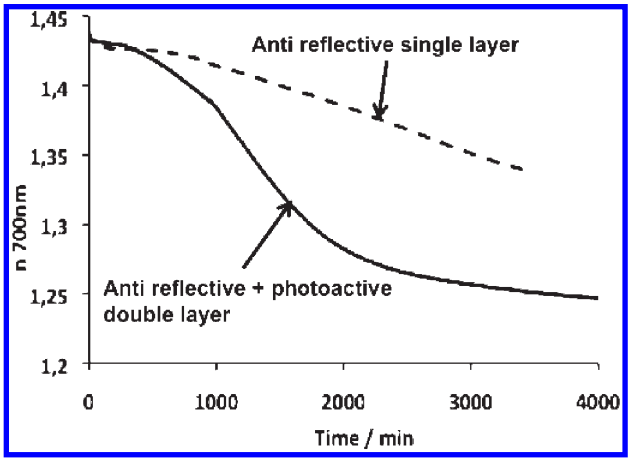

Figure 8. Evolution of refractive index with UV irradiation time for both single AR (AR2 sample) layer and AR-PA bilayer (AR2PA sample) systems contaminated with Lauric acid.

Young Modulus (E) to be around 1.5(±0.3) GPa. As the maximum film contraction observed upon capillary condensation is about 3% of the film initial thickness, we can conclude that the mesoporous hybrid AR layer is behaving mechanically very much like mesoporous purely inorganic ceramics.[19] Thus, organic functions introduced into the silica network are mainly located at the interface of the silica walls and do not weaken the silica framework beyond an acceptable point for the AR coating application. In addition, the bilayer system was resistant to cleaning with a soft tissue soaked either by water, ethanol, or acetone. The complete removal of the bilayer coating was achieved only after 5 cycles of aging 5 min in a concentrated KOH solution followed by rubbing with a dry tissue, confirming its relatively good mechanical stability.

Figure 7 shows the infrared absorption spectrum in the 4000−900 cm^{-1} range of a MTEOS−TEOS hybrid film that has been treated at 450 °C for 10 min and immediately increased to 500 °C for 5 min. The spectrum shows an intense absorption band peaking at 1050 cm^{-1} that is assigned to Si−O−Si antisymmetric stretching, which indicates the formation of the silica network. On the other hand this network appears well condensed because no signals due to silanols at 910 cm^{-1} (Si−OH stretching), and 3300 cm^{-1} (O−H stretching) can be observed. Two small bands at 3657 and 3765 cm^{-1} are assigned to the presence of tween (geminal) and isolated silanols, respectively, which are the residual of the condensation of silanol chains. This is in accordance with previous findings and is a good indication of the state of the surface upon condensation. On the other hand, the spectrum gives also some important information: no signals due to absorbed water are present, neither at 1640 cm^{-1} nor at 3200 cm^{-1} (O−H stretching), and a strong sharp signal at 1280 cm^{-1} indicates the presence of CH_3 groups in the film. The FTIR data indicates therefore that the film structure is formed by a well condensed silica network which is modified via the covalent Si−C bonds with methyl groups mainly located at the surface of the pores.[20−22] The fact that methyl groups were not fully decomposed at such high temperature is not yet fully understood but is likely due to the confinement and fast thermal treatment. The presence of these hydrophobic species avoids the absorption of water or other hydrophilic moieties from the external environment within the film.

(20) Innocenzi, P. *J. Non-Cryst. Solids* **2003**, *316*, 309.
(21) Malfatti, L.; Kidchob, T.; Falcaro, P.; Costacurta, S.; Piccinini, M.; Cestelli Guidi, M.; Marcelli, C.; Corrias, A.; Casula, M.; Amenitsch, H.; Innocenzi, P. *Microporous Mesoporous Mater.* **2007**, *103*, 113.
(22) Falcaro, P.; Grosso, D.; Amenistch, H.; Innocenzi, P. *J. Phys. Chem. B* **2004**, *108*, 10942.

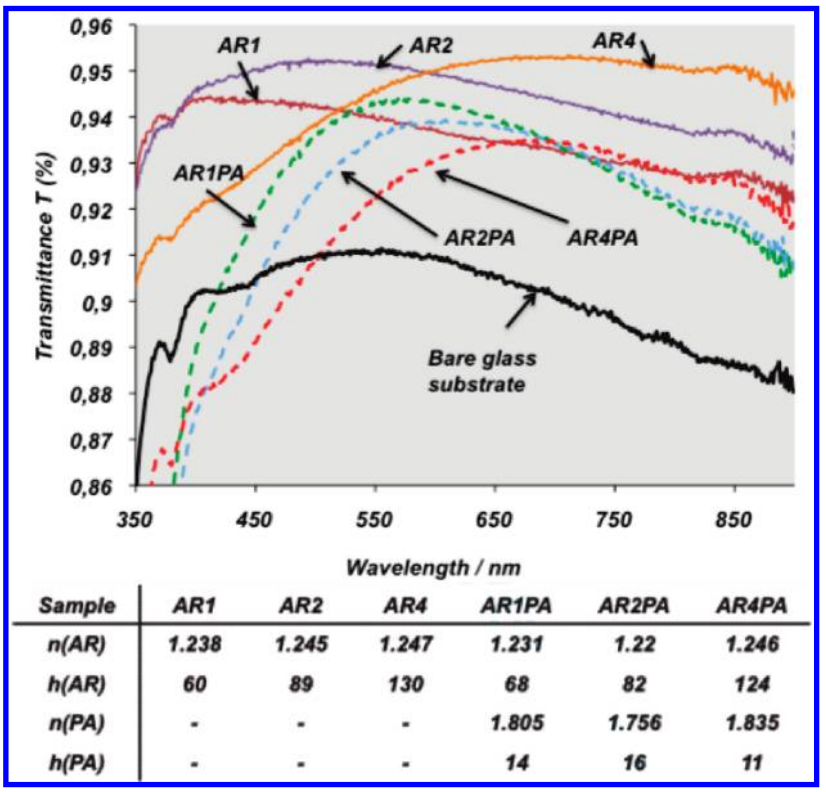

Sample	AR1	AR2	AR4	AR1PA	AR2PA	AR4PA
n(AR)	1.238	1.245	1.247	1.231	1.22	1.246
h(AR)	60	89	130	68	82	124
n(PA)	-	-	-	1.805	1.756	1.835
h(PA)	-	-	-	14	16	11

Figure 9. UV−visible analysis in transmission at 90° incident angle of the single layer (plain lines) and bilayer (dotted lines) systems deposited on one side of the glass microscope slide substrate. Thickness and refractive index (measured by ellipsometry) of each system are reported in the joint table.

Photocatalytic efficiency of both single AR layer and AR2PA bilayer systems was investigated by ellipsometry in situ during UV irradiation. The hydrophobicity of the pore permits to fill them up with Lauric acid pollutants. The contaminated system was then placed below a UV-lamp, and the variation of refractive index was recorded every minute by ellipsometry over a period of 3 days (see Figure 8). The initial thickness and refractive index of the AR layer before impregnation were 130 nm and 1.23, respectively. After impregnation with Lauric acid, the thickness does not change while the refractive index increases up to 1.43, suggesting that a fair proportion of the porosity volume was contaminated. While the AR2PA bilayer system regained its initial porous state after 2 days of irradiation, the TiO_2 free system has eliminated only less than 50% of its contamination by natural non-catalyzed UV decomposition for the same period, confirming the photocatalytic role of the TiO_2 PA top layer. Even if the TiO_2 is located outside of the AR layer, it provokes the photodecomposition of the Lauric acid molecules located inside the AR layer by ellipsometry, suggesting that contaminant species do not have to be in direct contact with TiO_2 to be eliminated. In this conditions, the decreasing of the refractive index is related to the decomposition of the Lauric acid presumably associated to the formation of $OH\cdot$ and $O_2\cdot$ radicals. The latter are produced as a result of the electronic transfer operating between the TiO_2 semiconductor surface and the adsorbed water upon irradiation. The products of the reaction between the radicals and the Lauric acid become more and more volatile and eventually evaporate from the film. For the bilayer geometry, one may state that Lauric acid diffuses toward the TiO_2 rich zone (surface), where irradiation is optimal and where the concentration of free radical is high. However, one cannot neglect the possibility that even if highly unstable, free radicals may have a sufficient lifetime to migrate inside the AR layer to decompose the pollutants.

Antireflective properties of both single AR layer and both AR-PA bilayer systems were assessed by UV−visible spectroscopy for different AR layer thickness. The percentages of transmitted light (transmittance) of AR, AR-PA, and substrate systems are plotted in Figure 9 in the visible wavelength range. In the inset table in Figure 9, one observes that the refractive index of the AR layer of the single and bilayer systems are close to 1.23 whatever the thickness. The PA layer has a refractive index and thickness close to 1.8 and 15 nm, respectively. As expected, the single AR coatings with a refractive index close to 1.23 provide the characteristic increase in transmission of around 4.5%, with a maximum transmission, corresponding to the first harmonic of the interference, shifting to higher wavelengths for higher thicknesses.

For the bilayer systems, the transmitted intensity is considerably decreased at lower wavelengths as a result of the anatase TiO_2 absorption below 350 nm. On the other hand, one notices that the antireflective properties are maintained in the visible range, reaching 3.5% gain at maximal transmission, even if they are slightly lower than that of the single AR layer systems. One can also observe that the maxima are shifted to higher wavelength because of the increase in optical path resulting from the presence of the TiO_2 layer. The latter results confirm that the bilayer

systems has efficient AR properties, resulting from the thinness and reduced refractive index of the PA top layer, and that the wavelength of maximum transmission can be adjusted by the thickness of the AR layer.

4. Conclusions

We have confirmed that antireflectivity, water-repellence, high wetting behavior (antifogging), photocatalytic activity (improved self-cleaning ability), and relatively high mechanical properties can be integrated into the same sol−gel coating made of a methyl modified SiO_2 and TiO_2 bilayer. The localization of the hard semiconductive TiO_2 ultrathin layer at the surface of the AR hydrophobic silica layer, provides (i) the surface high energy necessary for high wetting, (ii) the direct exposure to radiation and pollutants, and (iii) an improved resistance to abrasion. Chemical precursors used to produce such materials are relatively low cost while the dip-coating liquid deposition process is highly suitable to large-scale production. The system showed no alteration of the structure and the optical properties after 9 months immersion in water, making these coatings serious candidates for use as antireflective, self-cleaning top coating for photovoltaic cells.

Acknowledgment. D. Jalabert (Centre de Microscopie Electronique d'Orléans) is thanked for TEM analyses and Dr. Vasana Maneeratana for the language corrections. The authors also acknowledge funding provided by The TERAMAGSTOR program, the CNRS and the UPMC.